P7.2

A MODELING STUDY OF KATABATIC FLOWS OVER SLOPES WITH CHANGING SLOPE ANGLE

Craig Smith and Eric Skyllingstad
College of Oceanic and Atmospheric Sciences
Oregon State University

1. Introduction

Atmospheric conditions in mountain basins are controlled by a number of processes generated both locally and by synoptic scale weather systems. When synoptic conditions are relatively weak, for example during anticyclone periods, basin circulations often follow a diurnal cycle with upslope flow during the day when surrounding mountains are heated, and down slope flows in the nighttime when the same slopes are cooled. Down-slope flows transport dense air into mountain basins and contribute to stagnant conditions during the winter season by filling the basin with relatively cold air, enhancing the strong stratification generated by local radiative cooling.

Accurate prediction of down-slope flows is critical for predicting how basin circulations will evolve. However, because down slope flows are usually shallow and stratified, it is not clear if current mesoscale models are capable of simulating these flows with enough fidelity to accurately predict fluxes in and out of mountain basins. Furthermore, accurate simulation of terrain-induced atmospheric phenomena, such as slope flows, depends on how well terrain is resolved within the model. In some cases, inadequate terrain resolution can lead to an error in the depth and magnitude of drainage flows. For example, application of smoothing algorithms to complex terrain data in a model with inadequate resolution can lead to an increase in average terrain height in regions with steep slopes.

Corresponding author's address: Craig Smith, 104 Ocean Admin Bldg, Oregon State University, Corvallis, OR 97330, email: csmith@coas.oregonstate.edu

For katabatic flows (downslope flows forced by surface cooling), air parcels over a slope have a buoyant potential energy that is proportional to their height above the valley floor. Conversion of buoyant potential energy into kinetic energy is increased when terrain-smoothing algorithms increase the average terrain height by removing sharp terrain gradients without proper weighting. Consequently, terrain smoothing can lead to an over prediction of the katabatic flow magnitude.

An example showing how a typical smoothing scheme affects terrain at various resolutions is presented in Fig. 1, which shows an arbitrary cross-section through the Wasatch Range along the eastern edge of the Salt Lake valley floor. Terrain has been smoothed over using the Barnes (1964) objective analysis method (Xue et al, 2000) in the Advanced Regional Predictions System (ARPS) model initialization package, which does not conserve average terrain height. Effective terrain height along the slope is elevated by the Barnes analysis method as grid spacing is increased. Overall, the Barnes scheme increases the effective height of slopes in areas of concave terrain, which can strongly affect the dynamics of modeled slope flows.

Our main goal in this paper is to examine how changes in terrain shape affect katabatic flow properties. We compare mesoscale models of katabatic flows over a simple, uniform slope and a compound-angled slope to check the consistency of both models. These experiments allow us to examine how slope flow evolution is controlled by turbulence fluxes and how the flow adjusts to changes in slope angle. Finally, we examine the energy budget of slope flows by relating the flow evolution to the conversion of potential energy into kinetic energy.

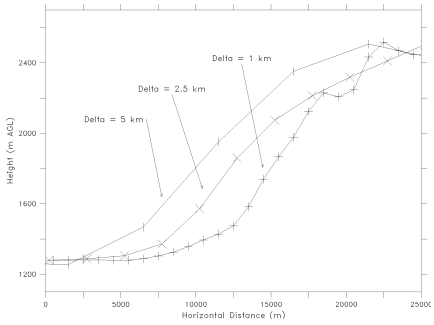

Figure 1. Terrain height (m) thru an arbitrary cross-section of the Wasatch Range along the eastern edge of the Salt Lake valley floor calculated using horizontal grid spacings of (a) 1, (b) 2.5, and (c) 5-km from the ARPS initialization package.

2. Model Setup

The mesoscale model used in our experiments is the Advanced Regional Prediction System (ARPS) described in Xue et al. (1999). ARPS is a nonhydrostatic, compressible model which utilizes a terrain-following coordinate system with a stretched vertical grid. Here, we used the model in a two-dimensional framework, representing a section across an infinite ridgeline. The model domain was 32 km by 0.6 km by 4 km in the *x, y* and *z* directions, respectively. Grid spacing was 100 m by 100 m in the horizontal with 320 grid points in the *x* direction and 6 grid points in the *y* direction. The terrain-following vertical coordinate was stretched to allow for a very fine grid size of 5 m near the surface where resolution is critical, expanding to 50 m well above the surface where flow variations were small. Eighty vertical levels were used spanning a total distance of 4 km with rigid top and bottom boundary conditions. Periodic boundary conditions were used in the cross-slope, *y* direction, while in the down-slope, *x* direction the boundary conditions were open (radiation). Simulations are forced with a constant surface cooling rate of 30 Wm^{-2}, radiation and moisture effects were not considered in our experiments. Surface roughness lengths were set to 0.01 m. The atmosphere was initialized at rest with a potential temperature of 18 ^{o}C. Simulations were conducted for one hour of model time, which was long enough for the katabatic flows to reach near steady state.

Simple (1 slope angle) and compound (two slope angles) slope comparisons utilized a linear terrain profile to focus specifically on the effect of terrain smoothing on katabatic flows. An *x-z* cross section of the model right-hand side slope for the compound and simple slopes is shown in Fig. 2. In our idealized example, the compound slope is considered representative of the 'true' terrain, including slope angle changes and sub-grid scale terrain features, while the simple slope is representative of smoothed-over and inadequately resolved terrain. This can be considered as representative of a smoothing scheme that reduced regions of steep slope angle by filling in valley side walls, a common result of typical smoothing schemes. For the purposes of this study, the simple slope is constrained to have the same horizontal distance and height as the compound slope. The lower- and upper-slope angles of the compound slope were set to α_1 = 1.6^0, and α_2 = 11.6^0, yielding an equivalent simple slope angle of α_s = 6.5^0. The total height of the compound and simple slope terrain was set to 822 m, giving a total horizontal run for the two slope scenarios of 7.3 km.

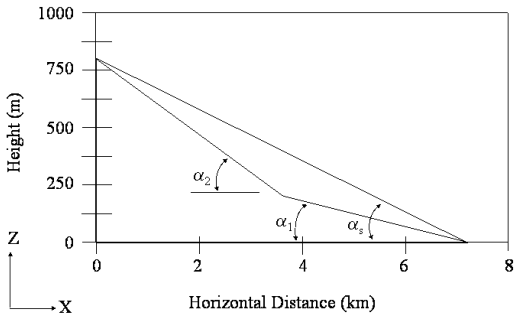

Figure 2. Cross section of a portion of the model domain for the simple/compound runs.

3. Results and Discussion

Cross section plots from the two simulations are presented in Fig. 3. A number of

distinct flow features are produced in the two scenarios. First, we note that except near the top of the slope, the uniform slope generates a stronger jet in comparison with the compound slope case. Slope flow depth, however, is greater for the compound case over the same slope region. Temperature deficit in the uniform slope case is less than the compound slope case, especially over the lower portion of the slope where the low angle slope in the compound case limits buoyant forcing of the flow. Weaker winds in the compound angle case limit the transport of cold air down the slope, leading to a greater temperature deficit.

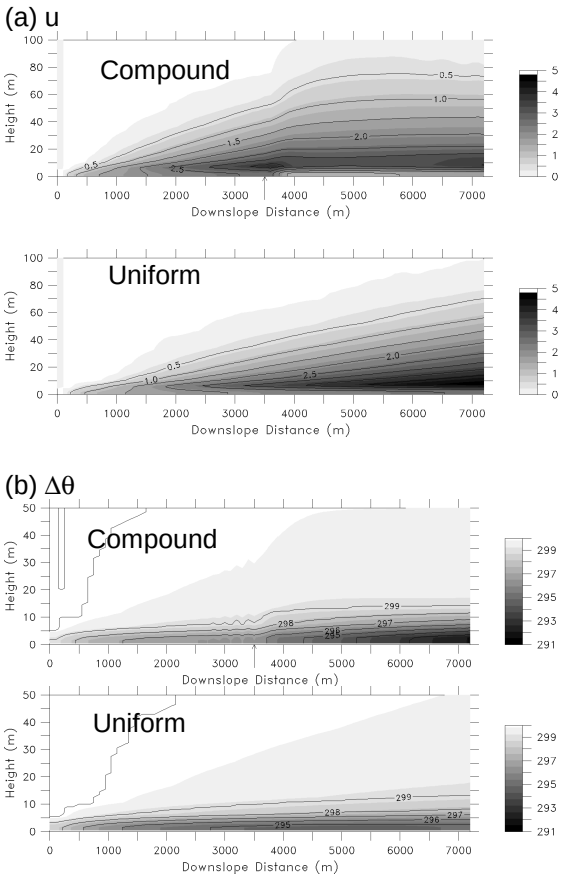

Figure 3. Cross sections (*x*-*z*) of (a) down-slope velocity, *u* (m s^{-1}) and (b) potential temperature deficit, $\Delta\theta$ (^{o}C), from the compound and uniform slope flows. The arrow indicates the location of the slope angle change.

A supercritical transition in the flow occurs in the flow in the region of the slope angle change. A plot illustrating the effect of transition period on the flow is presented in Fig. 4, which shows downslope velocity versus height 200 m before and after the change in slope angle for the compound angled case. This transition period consists of mass convergence and deepening of the flow, and as slight increase in the depth of the jet.

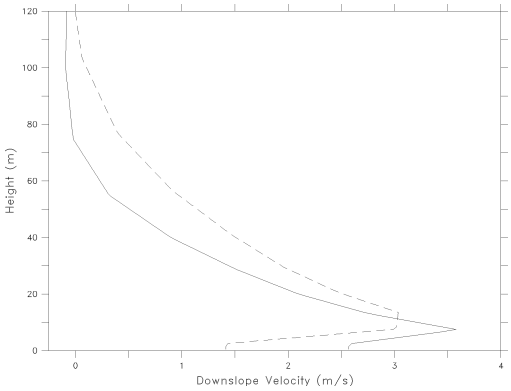

Figure 4. Plot of down-slope velocity, *u* (m s^{-1}) from the compound slope flows, 200 m before (solid) and after (dashed) the change in slope angle.

Because surface cooling rates are held constant, buoyancy deficits in the flow are largely controlled by flow velocity and slope angle. This has important implications for the momentum budget of the flow. The mean momentum equation in the down-slope direction, neglecting storage and the Coriolis term, may be written as in Mahrt (1982),

$$\sin\alpha\; g\frac{\theta'}{\theta_0} - \cos\alpha\frac{g}{\theta_0}\frac{\partial(\overline{\theta}h)}{\partial s} = \frac{\partial}{\partial n}K_m\frac{\partial u}{\partial n} - \left(u\frac{\partial u}{\partial s} + w\frac{\partial u}{\partial n}\right)$$

I II III IV

where the pressure gradient term has been rewritten using hydrostatic balance so that

$$\frac{1}{\rho_o}\frac{\partial p}{\partial x} = \cos\alpha \frac{g}{\theta_o}\frac{\partial(\bar{\theta}h)}{\partial x} \ .$$

The layer average potential temperature is defined as

$$\bar{\theta} = \frac{1}{h}\int_0^h \theta \, dz$$

and θ_0 represents a constant, reference potential temperature. Turbulent flux divergence is expressed as an eddy viscosity flux,

$$\frac{\partial}{\partial n}\overline{u'w'} = \frac{\partial}{\partial n} K_m \frac{\partial u}{\partial n}.$$

Following Mahrt (1982), terms in the momentum budget equation are grouped as follows. Term I is the sum of the buoyancy and pressure terms, including the katabatic acceleration, which is the primary driving force for the flow. Term II is the thermal wind term, which represents a retarding factor due the down-slope increase in stability. For the flows presented here, the thermal wind term is much smaller than the katabatic acceleration term. Term III is the sum of turbulent mixing and surface drag, which is included as a boundary condition. Term IV is the sum of the down-slope and slope-normal advection terms, and represents the horizontal advection of lower momentum from up-slope.

Previous studies, such as Nappo and Rao (1987), indicate that the bulk velocity magnitude of katabatic flows is a strong function of slope angle as indicated by term I of the momentum equation. Therefore, in the compound slope angle case it's reasonable to expect a flow transition when going from the high to low angle sections of the slope as shown by Fig. 3 (assuming the flow is near equilibrium). Forces acting on air parcels moving through the slope angle transition change suddenly, with term I decreasing rapidly thru the change in slope angle. To maintain balance between the momentum budget terms, the flow can either lose momentum via vertical mixing and surface drag (increasing term III) or undergo a reduction in the advection magnitude (term IV). Figure 3 suggests that both of these mechanisms are active in the compound slope flow case; the depth of the flow increases more rapidly and the strength of the near surface jet decreases so that the surface drag is smaller. Reduced surface velocity also decreases the downslope advection term (IV) downstream from the angle change.

Plotting the vertically averaged mixing and drag term (III) normalized by buoyancy (I) provides a more direct example of this effect (Fig. 5). For most of the slope flow, the vertical mixing and drag term balances about 70% of the buoyancy forcing. When the slope angle changes, the buoyancy term decreases rapidly to the point where term III is larger than term I. Adjustment occurs as the flow depth increases and the near surface velocity decreases between *x* = 3500 and 4500 m. Slower down slope velocities also increase the potential temperature deficit because the air has more time to cool before advecting down slope.

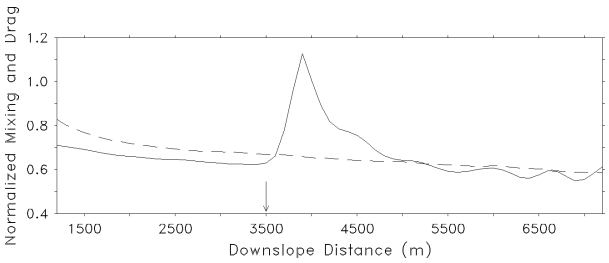

Figure 5. Vertically integrated normalized mixing and drag versus down-slope distance for the compound (solid) and simple (dashed) slope flows.

4. Energetics of Slope Flows

Effects of slope angle changes are made clearer by examining the total energy budget of the flow system. In slope flows, the source of total kinetic energy is gravitational potential energy, defined here as a flow depth average,

$$PE = \int_{h}^{h+150} zg\frac{\theta'}{\theta_o}dz,$$

where *h* is the slope height above the valley floor and the integration is performed to 150 m above the local surface. Similarly, we define the depth average total kinetic energy as

$$KE = \int_{h}^{h+150} \frac{1}{2}\left(u^2 + v^2 + w^2\right)dz.$$

Katabatic flows are generated when buoyant potential energy is added to the system through surface cooling and converted into kinetic energy. Kinetic energy is lost primarily via surface drag and dissipation of turbulence. Plots of *PE* and *KE* from the uniform slope ARPS case (Fig. 6) demonstrate how the total energy is partitioned along the slope. Near the top of the slope, *PE* climbs rapidly to a maximum while the *KE* field slowly increases from the initial state of no motion. Rapid growth of *PE* is produced by the relatively high altitude of the slope and the limited amount of time available for the slope flow to accelerate. For an equilibrium slope flow in a neutral atmosphere, the down hill flux of heat at any point along the slope must equal the total heat lost to the surface along the slope above the point. Near the top of the slope, the down slope velocities are relatively weak, consequently the temperature deficit must be large to yield a down hill heat flux equal to the total surface heat loss.

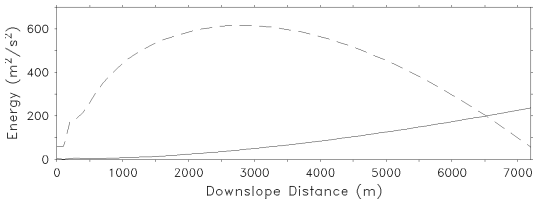

Figure 6. Vertically integrated total kinetic energy (solid) and buoyant potential energy (dashed) versus down-slope distance for the uniform slope case.

Moving down the slope, *PE* decreases as *KE* increases, so that the flow eventually has an equal energy partition at *x* = ~6500 m. Figure 6 shows that *PE* decreases more rapidly than the increase in *KE* in the lower half of the slope. Energy loss from surface drag and turbulence dissipation prevents the total *KE* from balancing the decrease in *PE*. At the bottom of the slope, *KE* reaches a maximum that is about 1/3 of the maximum *PE* value on the upper slope, indicating that about 33% of the available *PE* is converted to *KE* for a 6.5^o slope.

Examination of the *PE* and *KE* fields from the compound angle case shows how important slope angle is in determining the available energy for down slope flows (Fig. 7). In the compound angle case, *PE* increases more slowly at the top of the slope in comparison with the uniform slope case. This is because the slope height is decreasing more rapidly and *KE* is growing faster in the compound angle slope flow. By the time the flow reaches the change in slope angle, it has almost twice the *KE* as in the uniform slope angle case. However, the *PE* is much less in the compound case, which greatly affects the growth in *KE* down slope from the transition. Interestingly, *PE* in the transition zone down slope from the angle change increases slightly after having fallen from a peak value of ~300 at x = ~1500 m. The increase in *PE* results from the added vertical mixing of potential temperature, noted above, that occurs when the flow decelerates. More significant near surface cooling in the lower angle slope region also adds to the *PE*.

Because *PE* decreases more rapidly in the compound slope case, *KE* is unable to increase significantly down slope from the angle transition. In contrast, the uniform slope case KE continues to increase, reaching a value about 50% larger at the slope bottom than the compound angle case.

Higher *PE* in the uniform slope case ultimately leads to more *KE* at the base of the slope and a greater exchange of air between the top of the slope and the valley floor. A similar behavior can be expected in mesoscale simulations that use terrain smoothed without conserving the total terrain height. For example, in basin regions we would expect stronger slope flows in comparison with observations, which could have important implications for valley circulations and the transport of pollutants.

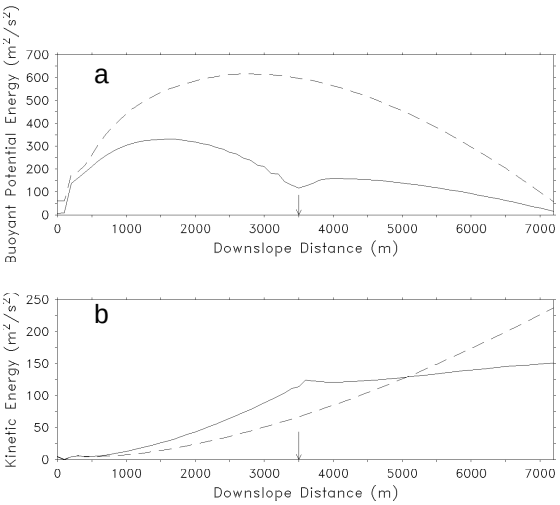

Figure 7. (a) Vertically integrated buoyant potential energy and (b) kinetic energy versus down-slope distance for the compound angle (solid) and uniform angle (dashed) slopes. The arrow indicates the location of the slope angle change.

5. Conclusions

Simulations of a compound angle slope are performed to demonstrate how changing slope angle can strongly affect the strength of down slope winds in katabatic flows. Slopes with a steep upper slope followed by a shallower lower slope (concave shape) generate a rapid acceleration on the upper slope followed by a transition to a slower evolving structure characterized by an elevated jet over the lower slope. In contrast, a case with uniform slope having the same total height change yields a more uniform slope flow profile with stronger winds at the slope bottom. Less available potential energy in the compound-slope case is shown to dramatically decrease the flow kinetic energy in comparison with the uniform slope example.

Our results show that the accuracy of katabatic flow predictions is inherently tied to terrain resolution within the model. Common ways in which terrain is smoothed in initialization packages can have the effect of reducing slope angle without conserving the average terrain height. For example, slopes with a concave shape may be filled as a means of maintaining the effective barrier height of a mountain range (e.g. Coupled Ocean/Atmosphere Mesoscale Prediction System, Chen et al., 2003). Terrain smoothing that does not conserve the average terrain height can cause an increase or decrease in production of potential energy available for slope flows. The net effect is unrealistic slope flow predictions that can produce large errors in valley and basin circulations. Our results suggest that terrain initialization methods should strive to maintain the average terrain height. If maintaining blocking height is important, then surface fluxes may need to be weighted to account for smoothed terrain having a larger effective height than the actual terrain.

Acknowledgements: This work was supported by the DOE Office of Biological and Environmental Research Environmental Meteorology Program.

6. References

Barnes, S. 1964: A technique for maximizing detail in numerical map analysis. *J. Appl. Meteorol.*, **3**, 395-409.

Chen, S., J. Cummings, J. Doyle, R. Hodur, T. Holtt, C.S. Liou, M. Liu, J. Ridout. J. Schmidt, W. Thompson, A. Mirin, and G. Sugiyama, 2003: COAMPS version 3 model description - general theory and equations. Naval Research Laboratory Technical Report, NRL/ PU7500-04-448. 141 pp.

Doran, J.C., and T.W. Horst, 1983: Observations and models of simple nocturnal slope flows. *J. Atmos. Sci*., 40, 708-717.

Horst, T.W., and J.C. Doran, 1986: Nocturnal drainage flow on simple slopes. *Boundary-Layer Meteor*., 34, 263-286.

Mahrt, L., 1982: Momentum balance in gravity flows. *J. Atmos. Sci*., 39, 2701-2711.

Manins, P.C., and B.L. Sawford, 1979a: A model of katabatic winds*. J. Atmos. Sci*., 36, 619-630.

Nappo, C. J. and S. Rao, 1987: A model study of pure katabtic flows. Tellus, 39A, 61-71.

Xue M, Droegemeier K, Wong V, 2000: The Advanced Regional Predictoin Systerm (ARPS) – A multi-scale nonhydrostatic atmospheric simulation and prediction model. Part I: Model dynamics and verification. *Meteorology and Atmospheric Physics*, 75, 161-193